Ocean Engineering 104 (2015) 511–520

Contents lists available at ScienceDirect

Ocean Engineering

journal homepage: www.elsevier.com/locate/oceaneng

Three-dimensional deformation of a large circular flexible sea cage in high currents: Field experiment and modeling

Pascal Klebert [a,*], Øystein Patursson [b], Per Christian Endresen [a], Per Rundtop [a], Jens Birkevold [a], Heini Winthereig Rasmussen [b]

[a] SINTEF Fisheries and Aquaculture, 7465 Trondheim, Norway
[b] Fiskeaaling, Aquaculture Research Station of the Faroes, Við Áir, FO-430 3 Hvalvík, Faroe Islands

ARTICLE INFO

Article history:
Received 18 September 2014
Accepted 19 April 2015
Available online 15 June 2015

Keywords:
Porous flexible structure
Current reduction
Fluid–structure interaction
In situ measurement
Eulerian current meters
3D dynamic super-element formulation
simulation

ABSTRACT

This paper presents the full-scale measurements of the deformation and current reduction of a large-scale fish sea cage submitted to high currents. Pressure tags were used to measure the cage deformation and the vertical displacement of the bottom ring, while an Acoustic Doppler Current Profiler (ADCP) and Acoustic Doppler Velocimeter (ADV) were used to measure the current reduction. The results show a reduction of 30% of the cage volume for current velocity above 0.6 m/s. The measured current reduction in the cage was 21.5%. A simulation model based on super-elements describing the cage shape was applied, and the results show good agreement with the cage deformations. Also the current flow measurements show the interaction between the sea cage and the bathymetry chart.

1. Introduction

The shift towards salmon farming at more exposed locations has been an industry-wide trend in Norway for the past decade. Moving fish farms to areas where high currents and waves exist can improve production through providing more stable temperatures and water quality and reducing the environmental impacts of modern fish farming (Holmer, 2010). However, exposed environments create challenges for salmon farming. If high currents and waves result in flows that exceed the typical swimming speeds of salmon, they may reduce the effectiveness of production. In addition, net deformation is often significant at exposed locations (Lader et al., 2008), which greatly reduces the space available for fish. Fish welfare is highly dependent on both the internal volume of the net structure and the hydrodynamic conditions. Thus, the synergistic effects of fast swimming in elevated flows generated by high waves and strong currents and reduced net volumes may prove particularly challenging for fish.

Nearly all cages in use for exposed farming in the Norwegian salmon industry are “gravity” type cages, according to the classification scheme proposed by Loverich and Gace (1998). These cages have a surface collar structure from which a net is hung within the water column. Gravity cages do not have rigid nets, and “bagging” deformation occurs during high currents, thereby decreasing the total cage volume. The force acting on the structure due to the fluid flow will affect the shape of the structure. Cages deform in current flow largely through lifting of the bottom netting and deformation of the front and back walls (Aarsnes et al., 1990; Løland, 1991, 1993). Current speeds of 0.13–0.35 m/s at two full-scale farms caused cage volume reductions of up to 20–40% and resulted in the cage bottom being pushed upwards (Lader et al., 2008). In extreme cases, where nets were severely deformed during storms that generated strong currents >1 m/s, mass mortalities of up to 40 tons of fish in a cage have occurred (Steine, 2004). Furthermore, in an aquaculture application, the internal volume of the net structure influences fish health and well-being, and therefore it is important to study how the volume reduction changes due to hydrodynamic force exposure. Flow through and around a cage is influenced by factors such as cage design, cage layout, fish movements, flow conditions at a site, and local topography (Klebert et al., 2013), but descriptions of these patterns and their correlations have not been field-tested. Simulations and lab-scale experiments have suggested that current speeds and net porosities can affect the internal hydrodynamics of sea cages (Shim et al., 2009; Gansel et al., 2008). The Norwegian government has introduced a new classification system (NAS, 2009) for fish farm sites using significant wave height and current speed (Table 1).

Current flows introduce loads that deform net cages, altering the available volume for fish and influencing their swimming and possibly feeding behaviors. Shim et al. (2009) performed simulations on a model scale to investigate flows through and around farms; a complex flow pattern existed with maximum drag at lowest net porosity. However, no tests have simulated flows on a full scale and

* Corresponding author. Tel.: +47 9822 24 73; fax: +47 56 36 75 85.
E-mail address: Pascal.klebert@sintef.no (P. Klebert).

http://dx.doi.org/10.1016/j.oceaneng.2015.04.045
0029-8018/

with flexible nets. This is due mainly to the limitations of the numerical models, which are mesh-based (Eulerian) approaches and require a large amount of memory to perform full-scale simulations. Other models (Lader and Enerhaug, 2005; Zhao et al., 2007) have been super-elements based and have focused only on the net structures without accounting for the current flow. Another numerical approach based on the joint use of the porous-media model and the lumped-mass model (Bi et al., 2014a, 2014b) has been used to simulate lab-scale experiments. In this article, field measurements of volume reduction in a large-scale fish cage and current reduction inside and behind the cage are presented as well as a numerical method based on these super-elements are presented and used in order to simulate the deformation undergone by the fish cage. The simulation results are then compared to the field measurements for validation of the method.

2. Material and methods

Measurements of current velocity and net deformation were conducted at a commercial marine salmon farm close to Torshavn in the Faroe Islands (61.99°N, 6.76°W) over a period of approximately 4 months. The farm itself had eight circular cages 41 m in diameter and two cages 50 m in diameter with a depth of 12 m to the bottom ring (Fig. 1).

Table 1
Norwegian aquaculture site classification scheme for waves and currents.

Wave	H_s (m)	T_p (s)	Degree of exposure	Current	V_c (m/s)	Degree of Exposure
A	0.0–0.5	0.0–2.0	Small	a	0.0–0.3	Small
B	0.5–1.0	1.6–3.2	Moderate	b	0.3–0.5	Moderate
C	1.0–2.0	2.5–5.1	Medium	c	0.5–1.0	Medium
D	2.0–3.0	4.0–6.7	High	d	1.0–1.5	High
E	> 3.0	5.3–18.0	Extreme	e	> 1.5	Extreme

H_s: wave height; T_p: wave period; V_c: current speed.

The depth of the site is 20–30 m, with the shallower part on the side towards the land, and the total biomass at the site was 1320 tons. The net cage (solidity $Sn = 0.225$) that was used for these experiments had a diameter of 41 m and a lower depth of 12 m; it is a gravity plastic cage with a bottom weight ring of 50 tons Tables 2 and 3.

The site has 10 cages organized in a mooring grid, as shown in Fig. 1. The depth of the mooring grid is 6 m. In Fig. 2, a farm layout is shown. The current is dominated by tidal currents with a maximum speed of around 80 cm/s. The current moves in both directions along the mooring grid and is approximately constant with the depth. During the days with the strongest tidal current, the peaks were around 65 cm/s, and during the days with the weakest current speed, the peaks were around 40 cm/s.

2.1. Current measurements: ADV and ADCP

The current measurements were conducted with three current profilers, two 600 kHz Workhorse Sentinels from RD Instruments that measured the average current speed close to the cage, and a 600 kHz AWAC from Nortek placed around 250 m in front of the cage in order to measure the reference current velocity. In addition, two Vector Acoustic Dopler Velocimeters (ADV) from Nortek were located inside the cage at a depth of 6 m.

All current profilers were set up similarly with a time interval between each profiling of 120 s and a bin height of 2 m. The profilers sampled for 60 s for each ensemble. The time interval between the measurements for the ADVs was set to 240 s.

The profiler data were processed using the same time intervals as the ADVs and pressure sensors. Data points were used only when cleared by the standard processing routines of the profiler data, and spikes were removed from the data in each interval when data points were more than twice the standard deviation away from the mean of the sample in the intervals. The interval averages were used only when the maximum difference between data points in each interval was less than 0.2 m/s, more than 50% of the data points were good, all the profilers had accepted means at all depths, and the difference in speed between the three uppermost bins in the reference and the up-current profilers was less than 0.1 m/s. In addition, only data sets with a minimum current of 0.15 m/s in the northerly direction were used.

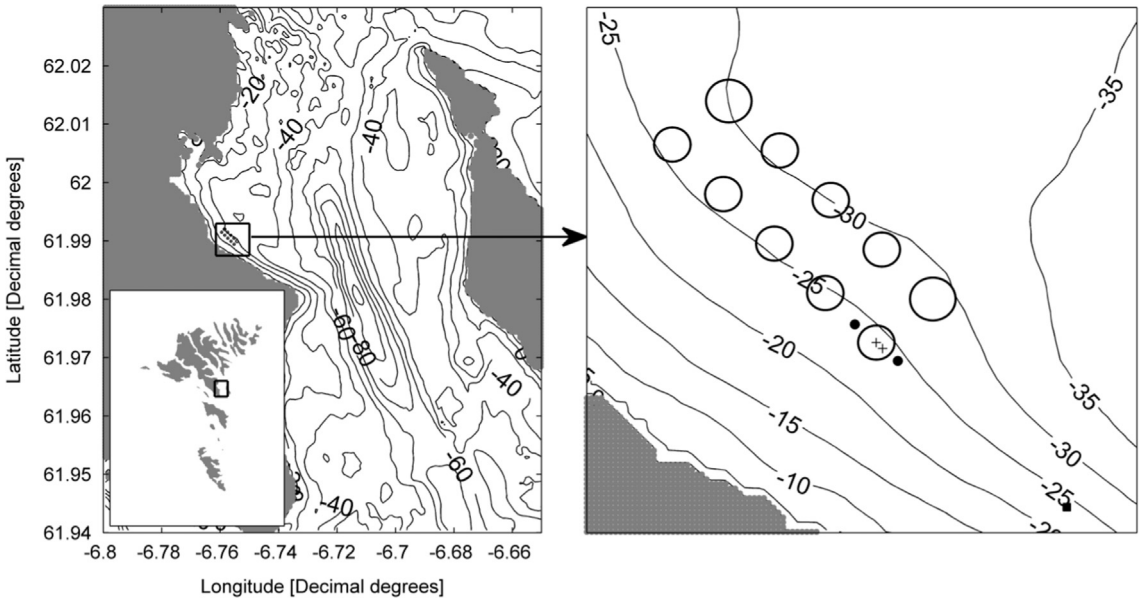

Fig. 1. Location of the farm in the Faroes.

Table 2
Fish farm specifications.

Cage	Circumference (m)	Depth side (m)	Depth center (m)	Weight ring (kg/m)
1	**128**	**12**	**20**	**50**
2	160	14	22	80
3	128	12	20	60
4	128	12	20	20
5	128	12	20	50
6	128	12	20	40
7	128	12	20	50
8	128	12	20	50
9	128	12	20	50
10	160	14	22	80

Table 3
Dimensions of the simulated net cage and support system.

Parameter	Value	Unit
Net		
Diameter	40.74	m
Height cylindrical part	12.0	m
Height conical bottom	8.0	m
Twine diameter	2.7	mm
Half mesh width	24.0	mm
Bottom weight	250	kg
Sinker tube		
Diameter center to center (c–c)	41.63	m
Pipe diameter	250	mm
Pipe wall thickness	22.7	mm
Initial depth	13.0	m
Submerged weight	50.0	kg m^{-1}
Floating collar		
Diameter (c–c)	41.64	m
Pipe radius	225	mm
Pipe wall thickness	25.6	mm
Distance between pipes (c–c)	0.9	m
Sinker tube chains		
Number	16	–
Length	13.0	m
Ropes sinker tube to netting		
Number	16	–
Length	1.097	m

In order to get an average vertical profile of the current at the three profiler positions, the mean values were normalized with respect to the average speed at the four uppermost bins at the reference profiler. The mean value of all the normalized speeds at each bin for each profiler was used for comparing the vertical profiles at the three locations. In addition to the profiler data, the ADV data were also normalized, and the average speed was compared to the profiler data as well. The average normalized speed from the profiler bins closest to 6 m depth and the average normalized speed from the ADVs were compared to investigate the velocity reduction with the distance through the mid-depth of the cage. These data are presented and discussed in Section 4.

Acoustic Doppler velocimeter (ADV): Twenty samples were measured every burst at a sampling rate of 1 Hz and a burst interval of 240 s. Fig. 3 shows an example of the data that were recorded over an interval of time during the total measurement period. It shows a pure tidal current from north to south and vice versa. From these measurements, the maximum current velocity $(U_{max})^i$, associated with a constant azimuth range, is extracted together with the corresponding time $(t_{max})^i$. The positions of the pressure tags are determined for the collection $(t_{max})^i$ in order to calculate the volume of the cage for a specific current velocity. The noise level was reduced by filtering the data with a moving average filter.

2.2. Deformation measurements and volume calculation with pressure tags

2.2.1. Measurements

The cage deformations were measured using pressure (depth) tags, which were mounted on several points on the cage (Fig. 4). This technique – but with a different type of pressure tags – has been used by Lader et al. (2008) with far fewer tags and for much smaller cages.

The pressure sensors were DST-milli tags, from Star-oddi in Iceland. DeCew et al. (2013) used a more advanced system (with receiver, pingers, and hydrophones) with a small cage, which allowed them to get live deformation data on the net. But this system is not used here as it required a substantial amount of receivers in order to overcome the effect of the important biomass in the large sea cage. These pressure sensors were located on the cage as shown in Fig. 4. Nineteen tags were attached around the net at different depths (2, 6, 12 m) and six around the bottom ring. A final sensor was used to measure air pressure so that the depth measurements could be corrected for air

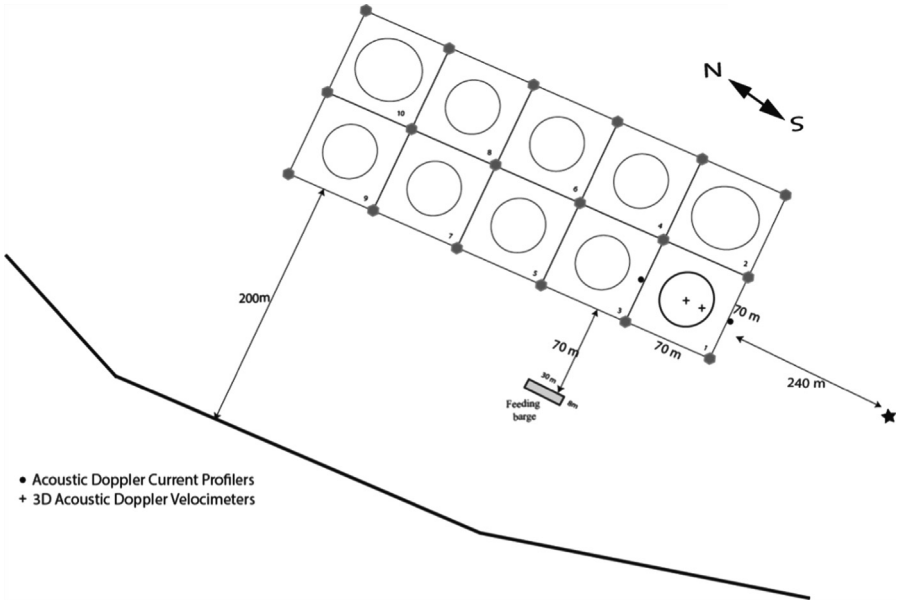

Fig. 2. Farm site layout and the locations of the sensors around the targeted cage.

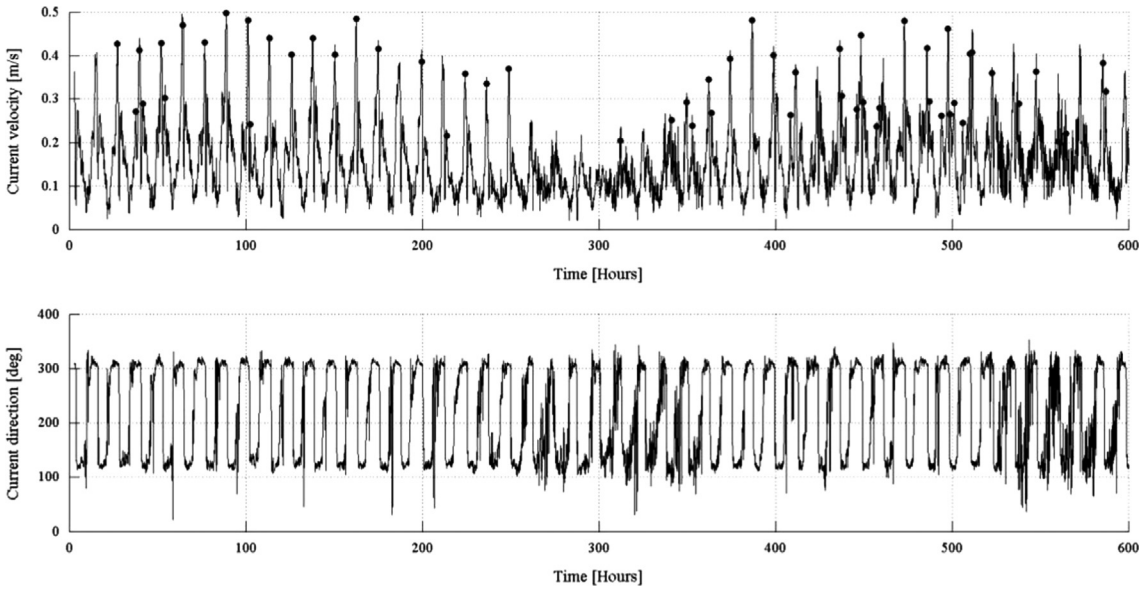

Fig. 3. Sample of current velocity profile from the ADVs in the cage: magnitude and azimuth.

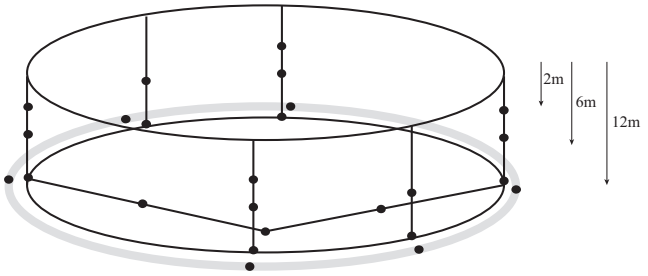

Fig. 4. Sketch of the cage with all the locations of the pressure tags on the net and the bottom ring.

pressure fluctuations. A special housing was used to fix these tags carefully to the nets. The depth range of these sensors is 0.1–20 m, with a depth accuracy of $\pm 0.4\%$.

The measurements from the depth sensors were processed to reduce noise by using a Finite Impulse Response (Lyons, 2010) low-pass filter with a cut-off frequency at 0.01 Hz in combination with a Matlab Zero-phase digital filtering algorithm (Mathworks, 2013). The pressure measurements were corrected for air pressure fluctuations measured by the air pressure reference sensor. The depth was calculated from the measured pressure under the assumption that it consists only of the static pressure ($P_{static}=\rho gh$, where ρ is the water density, g is the acceleration of gravity, and h is the depth). Corrections were made by assuming that the lowest (deepest) measurements that each sensor gave were equal to its theoretical "zero level", which happened when there was no current and so the net was undeformed. The time series was then shifted according to this to give the correct zero level. The *xyz* positions of each sensor for each time point were then calculated using the method described hereafter.

2.2.2. Cage volume calculation

To estimate the volume reduction in currents of different strengths, the *xyz* coordinates (hereinafter referred to as nodes) of the sensor array on the net cage were used. In addition, fixed nodes representing the floating collar connection points were also part of the collection. Because of the limited number of nodes, it was not possible to calculate the exact absolute volume of the net cage. Linear interpolation between nodes was used to form a grid to represent the inner cage volume from top to bottom.

- *Organizing the nodes*: In order to calculate the volume defined by the nodes, these needed to be sorted into layers. In addition, to have a clearly defined polyhedron, each node must be characterized by its immediate neighbors. This is done in the most intuitive way:
  - Each node can have a maximum of four connections (except the bottom node, which is connected to all in the layer above, and if there are different numbers of nodes in two neighboring layers, some nodes will have five connections).
  - Each node is connected to the nearest node on the right and the left as well as above and below.
  - The nodes in the top layer have three connections (none above).
  - The resulting polyhedron is assumed to be convex.
- Method for calculating the volume deformation. Two methods have been considered here:

2.2.2.1. The pancake method. This is similar than the method used in Lader et al. (2008): it only works in cases where there is an equal number of nodes in each layer (except for the bottom layer, where there is only one). The method is based on summing up volumes of pie pieces between each layer, and for the bottom layer there will be a sum of volumes of pyramids. The area of each pie piece in each layer is calculated and given a representative depth, then the volumes between corresponding pie pieces in two neighboring layers are calculated and summed up to give the total volume. The volume of each pie piece is calculated using the formula for the volume of a frustum (a pyramid where the top is cut off by a plane parallel to the base of the pyramid):

$$V=\tfrac{1}{3}h(A_{Top}+\sqrt{A_{Top}A_{Bottom}}+A_{Bottom}), \quad (1)$$

where h is the distance between the two planes, and A_{Top} and A_{Bottom} are the area of the upper and lower bases. The error of this method is mainly linked to the assumption that each pie piece is a frustum, which is not suitable for high deformation, but it gives a good estimate. Also, the height of each triangle is calculated as an average of the height of the three vertices, which may result in the loss of some information.

Therefore, another method, which finds the exact volume of the polyhedron and handles a different number of nodes in each layer, is introduced.

2.2.2.2. The polygon method. This method calculates the exact volume in the polyhedron (deformed sea cage) and is used later in this article. To calculate the volume, a plane parallel to the surface of the sea is defined at the height of the bottom node and another plane (parallel to the first) at the height of the second lowest node (Fig. 6). The volume of the polyhedron between these two planes can then be calculated as an upside-down pyramid with an irregular base area. Then the method proceeds with a plane being placed at the third lowest node (still parallel to the others). The second and third planes define a volume limited by the two cross sections (these are now irregular polygons), and in between there are only straight lines connecting pairs of corners of the polygons (some corners might have more than one line connected to them if there are different numbers of nodes in each layer). The area of the cross section defined by the intersection of the polyhedron and a plane moving between these two planes ($A1$, $A2$), will change as a second-degree polynomial.

To prove this, we can start by dividing the polygon into triangles. Then we have to prove that if the vertices of a triangle $\boldsymbol{u}$,$\boldsymbol{v}$ and $\boldsymbol{w}$ move along straight lines, the area of the triangle changes as a second-degree polynomial. The new vertices can be described as follows (Fig. 5):

$$\boldsymbol{u}' = \boldsymbol{u} + t \cdot \boldsymbol{n}_1, \quad \boldsymbol{v}' = \boldsymbol{v} + t \cdot \boldsymbol{n}_2, \quad \boldsymbol{w}' = \boldsymbol{w} + t \cdot \boldsymbol{n}_3, \tag{2}$$

where $\boldsymbol{n}_1$,$\boldsymbol{n}_2$ and $\boldsymbol{n}_3$ are vectors scaled so that the triangle stays in a plane parallel to the original triangle when t increases. The area of the triangle can be calculated as a cross product of vectors along the sides.

$$A_T = \tfrac{1}{2} \left| (\boldsymbol{v}' - \boldsymbol{u}')(\boldsymbol{w}' - \boldsymbol{u}') \right| \tag{3}$$

It is now easy to see that this will result in a second-degree polynomial of t, since we multiply two first-order polynomials, and this proves that the area changes as a second-degree polynomial. Now, since the area of the polygon is a sum of triangles, the area of the polygon will change as a second-degree polynomial.

$$A(x) = ax^2 + bx + c, \ \forall x \in [0, h]$$
$$A(0) = A_1, \quad A\left(\frac{h}{2}\right) = A_h, \quad A(h) = A_2 \tag{4}$$

Here, A_1 is the area of the lower cross section and A_2 is that of the upper, h is the height between the two planes, and A_h is the area of the cross section in the middle between the two planes. (A_h is required because more information is needed to find a, b, and c.)

To find the volume (Fig. 6), the area needs to be integrated between the two planes, resulting in

$$V = \int_0^h A(x)dx = \frac{1}{6}h(A_1 + A_2 + 4A_h) \tag{5}$$

Then the algorithm continues by adding a fourth plane at the height of the fourth lowest node and integrating the area between planes three and four and so on until the top is reached. The first step is actually a special case of the rest of the method with $A_1 = 0$.

The volume was calculated for each tidal cycle at the moment of the current peak measured by the ADV sensors. At this point, it was assumed that the maximum deformation had been obtained. The net cage deformation at each current peak was calculated as the percentage of undeformed volume:

$$\text{Deformation} = 100\left(1 - \frac{\text{current peak volume}}{\text{undeformed volume}}\right), \tag{6}$$

The undeformed volume was calculated when the current was approximately zero between each of the current peaks. In this article, only the polygon method is reported (Fig. 12), but the two methods have been compared, and a maximum deviation of $\pm 10\%$ can be reported.

3. Modelization

3.1. Theory

An investigation of the volume reduction of the net cage was also conducted using the numerical software tool FhSim developed at SINTEF (Reite et al., 2014). FhSim solves numerically mathematical models based on ordinary differential equations (ODEs) in the time domain, and it is a flexible and suitable program for analyzing flexible structures such as aquaculture gravity-type net cages. When simulating complex systems, the complete model is built up from several sub-models that communicate, for instance, their position, velocity, and tension or compression forces between each other through input and output ports. This enables the investigation of complex systems through a combination of simpler sub-models, which gives the flexibility needed to assess the effect of, for instance, design changes and alterations on aquaculture net cages.

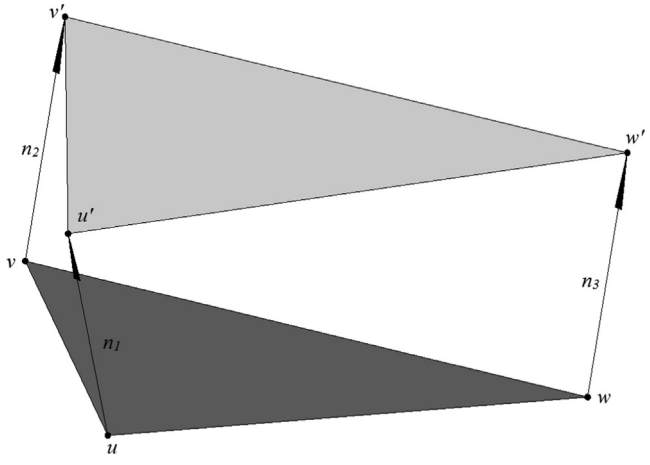

Fig. 5. Definition of the volume of a polyhedron between two planes.

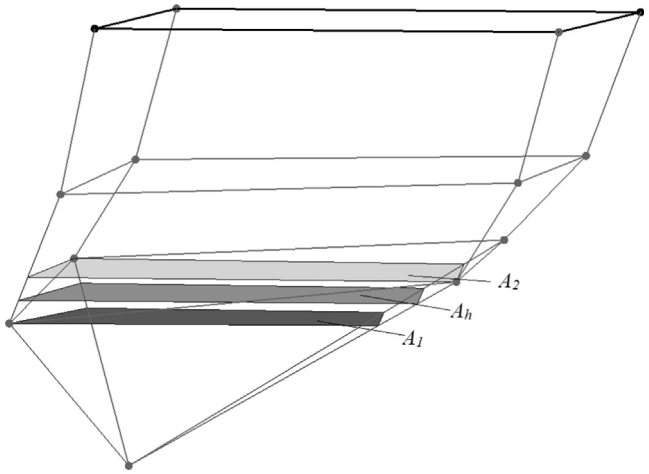

Fig. 6. Upward movement of the plane during the algorithm. The gray areas are the cross section.

The required model components consist of separate net elements and cable models representing ropes, a flexible floating collar, a sinker tube, chains, and anchor lines. Each model is responsible for calculating its own response due to external forces. These external forces are environmental forces (water current and waves) and forces induced by being connected to other parts of the structure. An example of the latter are the chains connecting the floating collar to the sinker tube: the cable model representing a chain will communicate its tension forces (forces at the two end points of the chain) to the floating collar and the sinker tube, which in turn will communicate their current position and velocity to the cable model.

For the modeling of the net cage system used during these measurements described in this study, numerical models for the net, floating collar, sinker tube, chains, ropes in the netting, and ropes connecting the net to the sinker tube in addition to mooring lines were developed. A detailed explanation of the net model and mathematical basis is given in Endresen et al. (2013, 2014) and Enerhaug et al. (2012). In the following, a brief overview of the principles and mathematical methods used in the net model is presented. Since estimation and evaluation of the net cage volume in currents, with the absence of waves, are of main interest, only a reference to the other sub-models is given as it is the net model that is of highest significance regarding the estimation of net volume reduction.

The net model is built up from a generic net structure, which gives the ability to simulate arbitrary complex net geometries such as trawls and aquaculture net cages or simpler structures such as varieties of net panels. Previously, the net model had been used to simulate net panels with rhombic meshes (Enerhaug et al., 2012), net panels with bending stiffness (Gansel et al., 2013; Jensen et al., 2013), and a variety of cylindrical net cages of smaller dimensions (Moe-Føre et al., 2014). The structural model of the net is based on Priour (1999, 2001, 2003). The net consists of triangular net elements (super-elements) that are interconnected through nodes in each of the three corners of each element. Environmental forces such as drag forces and wave excitation forces, external forces due to connection points with the sinker tube through the sinker tube ropes, and inertia and structural forces are divided between and lumped on the nodes. Thus, the external forces on the net and internal reaction forces of each element are realized through the nodes of the net structure. Hydrodynamic forces are found by using a Morison-type drag formulation.

Hydrodynamic forces are calculated for each triangular element in the numerical net structure. In the following, an overview of the steady forces from the water current will be given. Each element consists of a number of twines with a diameter and length. The length and diameter give the solidity ratio (Sn) for the net: Sn is the ratio between the projected area of the net material and the total area of the net panel. The incident water velocity for each panel – direction and magnitude – is used to calculate the forces exerted upon the element. Due to mass conservation, the water flow is accelerated through the mesh. The increased water velocity can, according to Kristiansen and Faltinsen (2012), be expressed as

$$u = \frac{\sqrt{2-Sn}}{\sqrt{2}(1-Sn)} U_0, \tag{7}$$

where u is the water velocity experienced by the net panel, and U_0 is the undisturbed incident water velocity. u and U_0 can be vectors, making the equation valid in three dimensions. The solidity ratio (Sn) is calculated using the formula $Sn = 2d_t/l_b$ and adjusted by a factor due to the reinforced intersection between twines, which increases the solidity ratio – d_t and l_b being the twine diameter and mesh bar length (half mesh), respectively. The incident water velocity is decomposed tangentially and perpendicularly to the twine bars in the element, and the calculated forces are mapped onto the global coordinate system. Twine bars in the net are treated as smooth cylinders, while the intersections between twines (knots) are represented by spheres. Adding up the contributions from all elements in the net model will yield the total force, in (x,y,z) coordinates, exerted on the net. Forces normal and tangential to each twine bar can be expressed as

$$F_{Nm} = \tfrac{1}{2}\rho d_t (l_b - d_k) N_B |u_N| u_N C_N, \tag{8}$$

$$F_{Tm} = \tfrac{1}{2}\rho \pi d_t (l_b - d_k) N_B |u_T| u_T C_T, \tag{9}$$

F_{Nm} and F_{Tm} are the normal and tangential forces on the net panel. ρ, d_k, and N_B are the water density, knot diameter, and number of bars in the element. u_N, u_T C_N, and C_T are respectively the normal and tangential velocity to the net panel twines and the normal and tangential drag coefficient of the twines in the netting. Each equation must be used twice, one for each of the two twine orientations. Forces exerted on the knots are given as

$$F_{Dk} = \frac{1}{2}\rho \pi \frac{d_k^2}{4} N_K |u| u C_K, \tag{10}$$

where N_K and C_K are the number of knots in the net panel and the knot drag coefficient (0.4). The normal drag coefficient is dependent on the mesh bar Reynolds number and set according to the polynomial presented in Kristiansen and Faltinsen (2012). For more details on the hydrodynamic load model for nets in FhSim, see Enerhaug et al. (2012).

The wake effect, meaning the reduction of incident water velocity due to blockage from upstream parts of the net is also included in the hydrodynamic load model in FhSim. The wake effect can be described

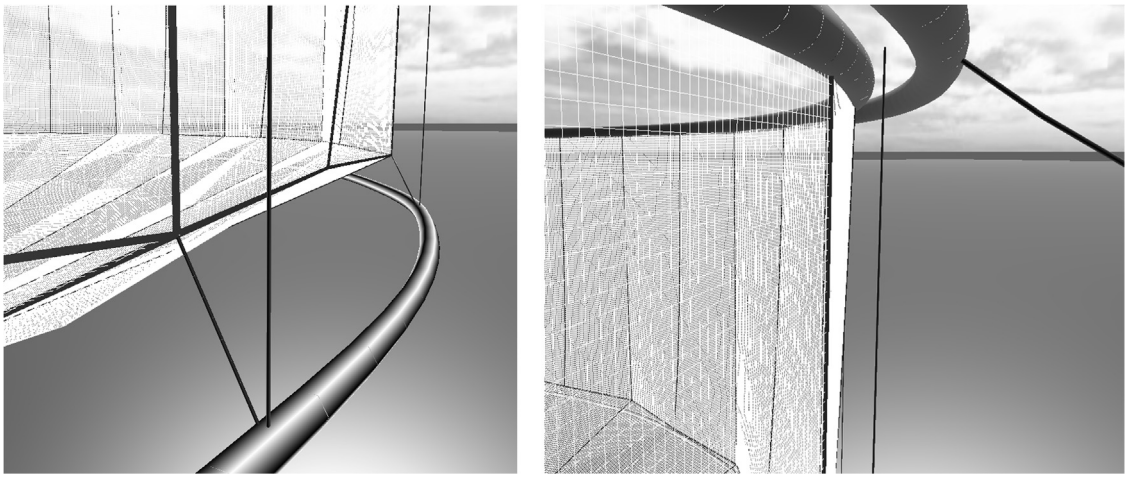

Fig. 7. Representation of the cage elements for the simulations.

as the change in water velocity downstream from an object placed in the water column and exposed to water current or towed through the water. In this article, the model developed by Blevins (2005) is used. Details regarding calculation of the wake effect are presented in Endresen et al. (2013).

Applied to the netting material of a net cage, this pertains to the change in water velocity downstream from the net. This means that the parts of the net being downstream from the other parts will experience a change in water velocity, in most cases a reduction, compared to the undisturbed flow. Modeling of this effect is important when estimating hydrodynamic loads on aquaculture net pens.

3.2. Simulations set-up

The net model consisted of 608 triangular net elements (super-elements), 16 side ropes, which continued as cross ropes in the net bottom, and 16 additional side ropes in the cylindrical part of the net. The net twine diameter, net half mesh width, and rope diameter were set according to the values given for the net used in the experiments. The net material itself was given a Young's modulus of 100 MPa, while the side ropes and cross ropes were given a Young's modulus of 1 GPa. The ropes connecting the net to the sinker tube were given a diameter and Young's modulus equal to 20 mm and 1 GPa, respectively, while the sinker tube chains connecting the floating collar to the sinker tube were modeled as steel cables with a diameter of 20 mm and a Young's modulus of 200 GPa. The net model had 32 connection points to the floater and 16 connection points to the sinker tube (through ropes), while 16 chains connected the floating collar to the bottom ring (Fig. 7). A simplified mooring system was used, consisting of two ropes at a 45° angle to the center line (water current direction) on the upstream side of the net cage and two ropes at a 45° angle to the center line at the downstream side of the net – this being a valid arrangement since the objective of the simulations is to model the effect on net cage volume due to a uniform constant current with respect to time and space. In order to determine the reduction of the volume enclosed by the net, a reference volume was created by running one simulation with a water current speed equal to zero: This enables the system, and especially the net, to stretch and settle, thus creating a more realistic reference than if the overall dimensions of the net cage were used.

4. Results and discussions

In this discussion section, only the data with the current direction from the south to the north are considered, as they affected the targeted cage first. The data of the current from the north are not discussed as this current is quite disturbed and is reduced in magnitude after passing through all the cages before the targeted cage.

4.1. Velocity reduction through the cage

The data from the profiler in front of the cage (Fig. 8b and e) and at the reference point (Fig. 8c and f) show quite a linear profile from the surface to the bottom with a constant flow direction: Only three different reference velocities are plotted, in order to illustrate the hydrodynamics in a simple way. The logarithmic behavior of the velocity field in the oceanic bottom (at −21 m) boundary layer can be seen as well (Fig. 8b and c): The thickness of this bottom boundary layer can be ranged till −16 m. 24 different profiles measurements for each current profiler and 12 corresponding measurements for the ADVs are plotted in Fig. 9 using the average normalized velocities; it shows that till the bottom of the cage, there is a reduction of the current speed with position from the reference profiler through the cage to the down-current profiler. At the same time, an increased velocity is observed in both Figs. 8 and 9 below the cage from the up-current to the down-current profiler, which is linked to the interaction with the bottom of the sea (−21 m): due to the presence of the system cage/biomass, the flow is partly deviated under it. This phenomenon will have a direct impact on the sedimentation process (feed pellets, feces, etc.) that usually occurs under sea cages.

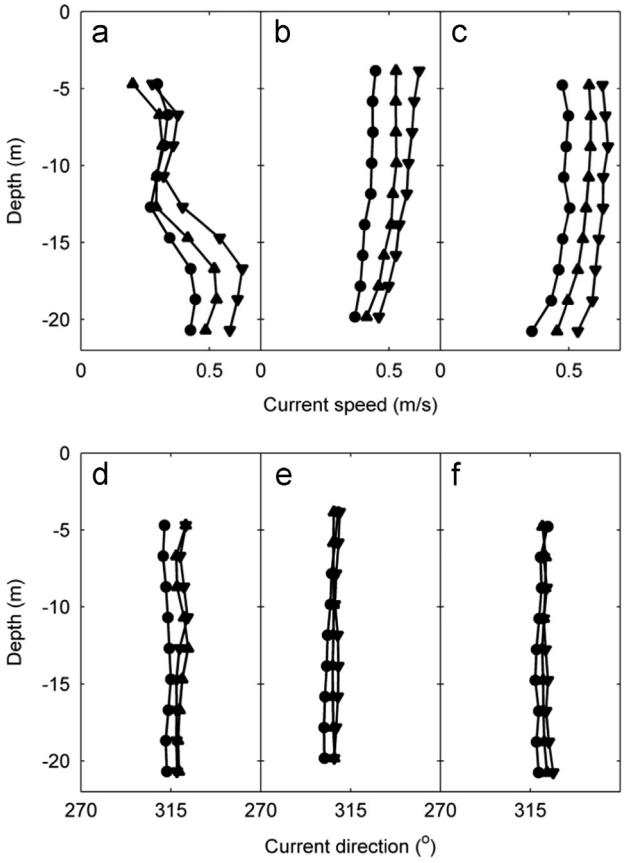

Fig. 8. Samples of vertical velocity profiles at the profiler down-current of the cage (a), the profiler up-current of the cage (b), and the profiler at the reference point (c). The profiles represent the slowest (circular points) and fastest (downwards pointing triangle) current speeds used for investigating the velocity reduction and one of the middle speeds (upwards pointing triangle).

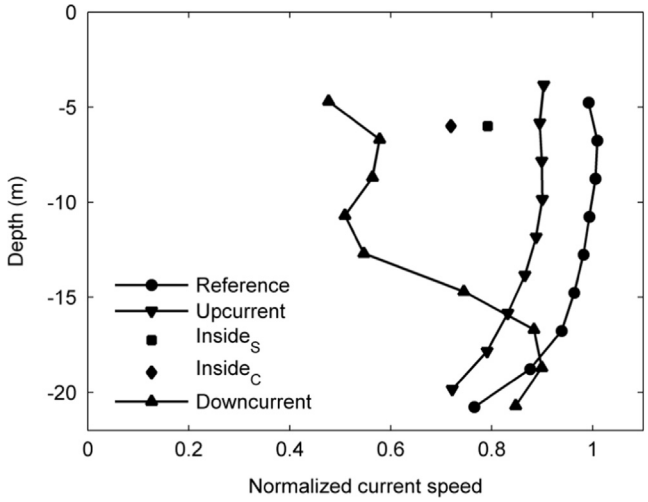

Fig. 9. Average velocities profile from the profilers around the cage and the reference point and average point velocities inside the cage.

The data points from the 6 m depth (Fig. 10) show a slight decrease in current speed from the reference to the up-current profiler and a much larger decrease in current speed through the cage. The velocity reduction through the cage is calculated from the data of the profiler in front of the cage and the velocity point measurements in the cage disposed along the diameter of the cage at the 6 m depth. The reduction from the reference to the up-current profiler was 11%, while the reduction through the cage – from the up-current to the down-current profiler – was 35%. The reduction from the reference point to the inside of the net cage was equal to 21.5%, which has to be compared with the value reported (reduction of 20%) by Løland (1991, 1993). Similar current reduction is also observed through the rear net of the cage. Only velocities data, from the sensors inside the cage, not affected by the fish are considered here. This velocity reduction differs to the one reported in Johansson et al. (2014) where the sensors in the cage were located in an area affected by both fish and nets during all the observed regimes, and so measured higher velocity reduction.

4.2. Volume reduction experiments and simulation

Water current velocities, ranging from 0.1 m/s to 1 m/s, were used for the simulation. The volume of the net cage was calculated according to the method presented in Section 2.2, with the positions of the nodes connecting the net elements used as input. Fig. 11 (a) represents the initial state of the cage with no currents and Fig. 11 (b) the deformation that occurs for a current speed of 0.5 m/s.

In these simulations, the total frame of the farm is not modeled, nor are the bridle lines, the anchors, and the buoys around the cage itself. Also, no sensitivity studies were conducted, in particular on the sinker tube, and the value for the bending stiffness was used according to the information gathered from the farmers at the site. The main focus is to study in which way this kind of super-element model can reproduce large-scale deformation of such structures. Fig. 12 represents a comparison of the cage volume deformation between the experiments and the simulation. As in Section 4.1, only the data from the south were considered as they provide the best clean direction current flow, which could be compared with the simulation. The overall comparison is good, but the simulation underestimates the measured deformation for low current velocities (0.2–0.3 m/s). Different reasons can explain this observation: The stiffness of the sinker tube may be overestimated so that it prevents deformation, some fouling on the nets was observed at some time periods, which correspond to these low velocities regime and which could lead to a larger deformation due to higher forces than the one calculated with the simulation; Also, the acceleration of the flow beneath the cage might amplify the deformation predicted by the simulation, which does not take into consideration the interaction with the bottom of the sea.

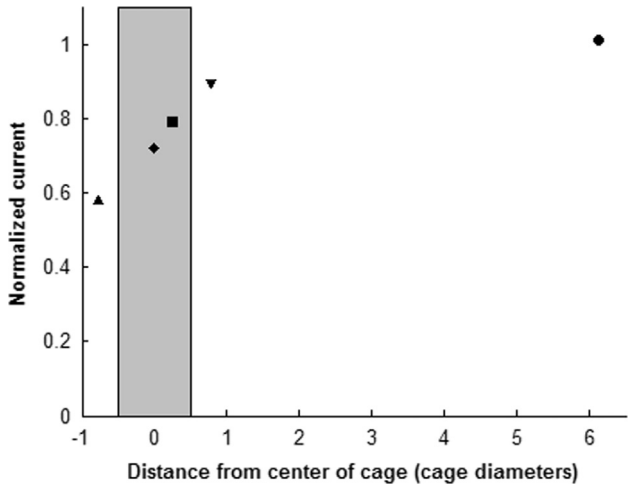

Fig. 10. Reduction of the flow through the cage. The markers are the same as those used in Fig. 9. The shaded area represents the cage position.

During these experiments, the force on the cage was not measured, so only the result from the simulation is reported in Fig. 13. This is compared to the drag on a square rigid cage using an empirical formula from Løland (1991, 1993) with and without a shadow effect (velocity reduction) on the rear net. By decomposing the hydrodynamic forces acting on a net panel due to a uniform current into normal and tangential force components and using the values proposed by Rudi et al. (1988) for lift and drag force coefficients, Faltinsen and Timokha (2009) proposed the following formulation for the normal drag of a net panel as a function of the angle (θ) between the incident low velocity and the normal vector of the net panel, the drag coefficient of a circular cylinder($C_D^{cylinder}$), the Reynolds number (Rn), and the Solidity (Sn) of the net.

$$C_D(\theta) = C_D^{cylinder}(Rn) \times \cos^2\theta \times \frac{Sn}{(1-Sn)^2}, \tag{11}$$

In Fig. 13, these different formulations are plotted. The two formulations from Løland are plotted for a square rigid net cage ($L \times l \times H = 40.74\ \text{m} \times 40.74\ \text{m} \times 12\ \text{m}$) as reported in his paper, and the formulation from Faltinsen is used for a circular rigid net cage (diameter = 40.74 m and height = 12 m). For all these three theoretical formulations, the bottom cone shape is not taken into account, unlike the simulation of these full-scale measurements, which might explain the lower force in comparison to the simulated one for low current velocity. For increasing current velocity, it can be seen that, unlike the theoretical formulations which are applied for rigid cages, the simulation curve follows a profile different from that of a square profile: This phenomenon is known as drag reduction by reconfiguration (Vogel, 1989, 2009; Delangre, 2008; Delangre et al., 2012) and has been quantified by using a

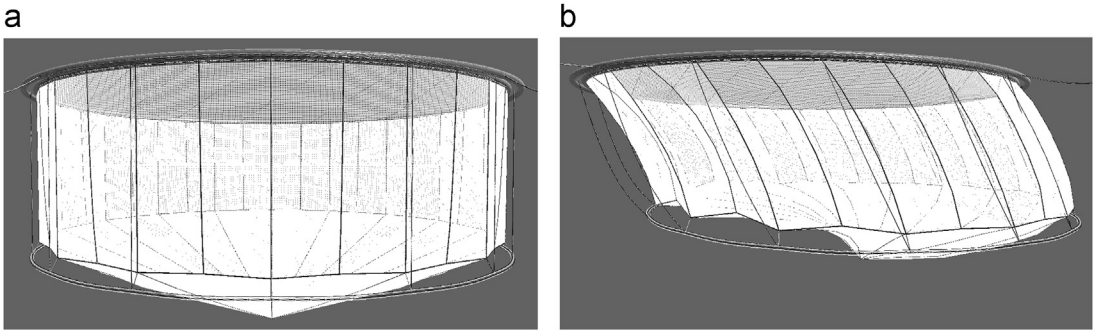

Fig. 11. Simulation of the deformation of the cage for current speeds: (a) initial volume for current speed = 0 m/s and (b) current speed = 0.5 m/s.

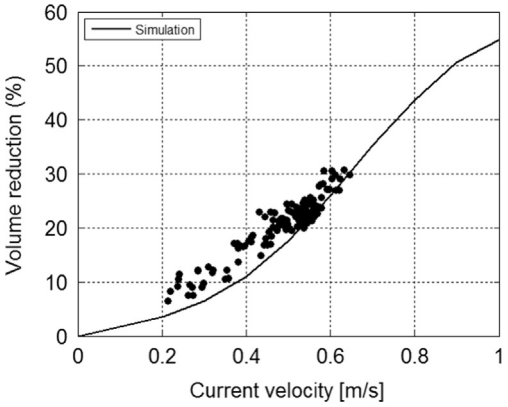

Fig. 12. Cage volume deformation: experimental and simulation results.

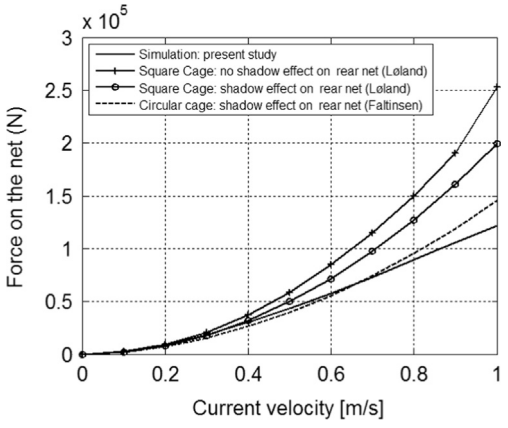

Fig. 13. Forces on the net of the cage: simulation results.

coefficient (Vogel's exponent) that measures the relationship between velocity and drag. In the present paper, neither a study on the mechanisms of reconfiguration by quantifying the change in shape and the size of the net cage and streamlines nor on building a mechanistic model of drag for reconfiguring for such a large-scale porous structure are performed.

5. Conclusions

In this study, 3D measurements of a large sea cage volume deformation and the current flow around and within the cage are presented. A reduction of 30% of the cage volume for a current velocity above 0.6 m/s is observed. The velocity profiles measured in front, within the cage, and at the back of the cage show the reduction of the current flow due to the presence of the cage. A reduction from the reference point to the inside of the net cage equal to 21.5% has been measured. Also an acceleration beneath the cage due to the interaction with the bottom of the sea is observed; this will influenced the sedimentation process (feed pellets, feces, etc.) which occurs under fish farm. In addition, a simulation based on super-elements was performed and quantitatively reproduces the measured cage deformation. Also, the computed force shows a profile that indicates that the drag grows in a less pronounced way than that of the classical square profile associated with bluff bodies. Overall, this study suggests that this simulation program could be used further to develop new cage concepts in order to prevent high deformation for optimum fish welfare.

Acknowledgments

This work was funded by the Norwegian Research Council through the research programs *Exposed Salmon Farming in High Current and Waves* (207116/E40) and *Towards Sustainable Fish Farming at Exposed Marine Sites* (210794/O70).

References

Aarsnes, J.V., Rudi, H., Loland, G., 1990. Current forces on cage, net deflection, Engineering for Offshore Fish Farming. Thomas Telford, London, pp. 137–152.

Bi, C.W., Zhao, Y.P., Dong, G.H., Zheng, Y.N., Gui, F.K., 2014a. A numerical analysis on the hydrodynamic characteristics of net cages using coupled fluid–structure interaction model. Aquac. Eng. 59, 1–12.

Bi, C.W., Zhao, Y.P., Dong, G.H., Zheng, Y.N., Gui, F.K., 2014b. Numerical simulation of the interaction between flow and flexible nets. J. Fluids Struct. 45, 180–201.

Blevins, R.D., 2005. Forces on and stability of a cylinder in a wake. J. Offshore Mech. Arct. Eng. 127 (1), 39–45.

DeCew, J., Fredriksson, D.W., Lader, P.F., Chambers, M., Howell, W.H., Osienki, M., Celikkol, B., Frank, K., Høy, E., 2013. Field measurements of cage deformation using acoustic sensors. Aquac. Eng. 57, 114–125.

De Langre, E., 2008. Effects of wind on plants. Annu. Rev. Fluid Mech. 40, 141–168.

De Langre, E., Gutierrez, A., Cossé, J., 2012. On the scaling of drag reduction by reconfiguration in plants. C. R. Méc. 340 (1–2), 35–40.

Endresen, P.C., Føre, M., Fredheim, A., Kristiansen, D., Enerhaug, B., 2013. Numerical modelling of wake effect on aquaculture nets. In: Proceedings of the 32nd International Conference on Ocean, Offshore and Arctic Engineering. OMAE 2013, Nantes, France.

Endresen P. C., Birkevold J., Føre M., Fredheim A., Kristiansen D., Lader P. (2014). Simulation and validation of a numerical model of a full aquaculture net-cage system. 33rd International Conference on Ocean, Offshore and Arctic Engineering Volume 7: Ocean Space Utilization; Professor Emeritus J. Randolph Paulling Honoring Symposium on Ocean Technology. ASME Press.

Enerhaug, B., Føre, M., Endresen, P.C., Madsen, N., Hansen, K., 2012. Current loads on net panels with rhombic meshes. In: Proceedings of the ASME 2012 31st International Conference on Ocean, Offshore and Arctic Engineering, vol. 7, pp. 49–60.

Faltinsen, O., Timokha, A., 2009. Sloshing (eq in p 282). Cambridge University Press, Cambridge.

Gansel, L., Jensen, Ø., Endresen, P.C., Føre, M., 2013. Deformation of nets with bending stiffness normal to uniform currents. In: Proceedings of the ASME 2013 32nd International Conference on Ocean, Offshore and Arctic Engineering.

Gansel, L., McClimans, T.A., Myrhaug, D., 2008. The effects of the fish cages on ambient current. In: Proceedings of the 27th International Conference on Offshore Mechanics and Arctic Engineering (OMAE2008), Estoril, Portugal.

Holmer, M., 2010. Environmental issues of fish farming in offshore waters: perspectives, concerns and research needs. Aquacult. Environ. Interact. 1, 57–70.

Jensen, Ø., Gansel, L., Føre, M., Endresen, P.C., Reite, K.J., Jensen, J., Lader, P., 2013. Oscillation of a net panel with bending stiffness. In: Proceedings of the 32nd International Conference on Ocean, Offshore and Arctic Engineering, OMAE 2013, Nantes, France.

Johansson, D., Laursen, F., Fernö, A., Erik, J., Klebert, P., Stien, L., Vågseth, T., Oppedal, F., 2014. The Interaction between Water Currents and Salmon Swimming Behaviour in Sea Cages. PLoS ONE 9 (5), e97635 http://dx.doi.org/10.1371/journal.pone.0097635.

Klebert, P., Lader, P., Gansel, L., Oppedal, F., 2013. Hydrodynamic interactions on net panel and aquaculture fish cages: a review. Ocean Eng. 58, 260–274.

Kristiansen, T., Faltinsen, O.M., 2012. Modelling of current loads on aquaculture net cages. J. Fluids Struct. 34, 218–235.

Lader, P., Dempster, T., Fredheim, A., Jensen, Ø., 2008. Current induced net deformations in full-scale cages for Atlantic salmon (*Salmo salar*). Aquac. Eng. 38, 52–65.

Lader, P., Enerhaug, B., 2005. Experimental investigation of forces and geometry of a net cage in uniform flow. IEEE J. Ocean Eng. 30 (1), 79–84.

Loverich, G.F. & Gace, L. 1998. The effect of currents and waves on several classes of offshore sea cages. In C.E. Helsley, (ed.). *Open Ocean Aquaculture '97, Charting the Future of Ocean Farming - Proceedings of an International Conference*. April 23-25, 1997, pp. 131–144. Maui, Hawaii, USA.

Løland, G., 1991. Current Forces On and Flow Through Fish Farms (Ph.D. thesis). NTNU, Trondheim, Norway.

Løland, G., 1993. Current forces on and water flow through and around, floating fish farms. Aquac. Int. 1, 72–89.

Lyons, R.G., 2010. Understanding Digital Signal Processing, third ed. Prentice Hall, ISBN-10: 0137027419. ISBN-13: 978-0137027415.

Mathworks, 2013. ⟨http://www.mathworks.se/help/signal/ref/filtfilt.html⟩.

Moe-Føre, H., Endresen, P. C., Aarsæther, K. G., Jensen, J., Føre, M., Kristiansen, D., Fredheim, A., Lader, P., Reite, K.-J., 2014. Structural Analysis of Aquaculture Nets: Comparison and Validation of Different Numerical Modelling Approaches. ASME 2014 33rd International Conference on Ocean, Offshore and Arctic Engineering, American Society of Mechanical Engineers.

NAS, 2009. NS 9415 Marine Fish Farms – Requirements for Site Survey, Risk Analyses, Design, Dimensioning, Production, Installation and Operation. ICS 65.150;67.260. Standards Norway, Norway. ⟨http://www.standard.no⟩.

Priour, D., 1999. Calculation of net shapes by the finite element method with triangular elements. Commun. Numer. Methods Eng. 15, 757–765.

Priour, D., 2001. Introduction of mesh resistance to opening in a triangular element for calculation of nets by the finite element method. Commun. Numer. Methods Eng. 17, 229–237.

Priour, D., 2003. Analysis of nets with hexagonal mesh using triangular elements. Int. J. Numer. Methods Eng. 56, 1721–1733.

Reite, K.-J., Jensen, J., Aarsæther, K.G., Føre, M., Endresen, P.C., Kristiansen, D., Kyllingstad, L.T., Rundtop, P., Johansen, V., Fredheim, A., 2014. Fhsim – a time domain simulation of marine systems, in: Proceedings of the ASME 2014 33rd International Conference on Ocean, Offshore and Arctic Engineering. http://dx.doi.org/10.1115/OMAE2014-23165.

Rudi, H., Løland, G.L., Furunes, L., 1988. Model Tests With Net Enclosures. Forces On and Flow Through Single Nets and Cage Systems. Technical Report, 513039.00.01.88, MARINTEK, MTC, Trondheim, Norway, 1988.

Shim, K., Klebert, P., Fredheim, A., 2009. Numerical investigation of the flow through and around a net cage. In: Proceedings of the ASME Conference, 2009, 581, doi: 10.1115/OMAE2009-79960.

Steine, J.-E., 2004. Vurderer mulkt etter laksedød. Altaposten (19/10/2004). ttp://www.altaposten.no/nyheter/article6785.ece (in Norwegian).

Vogel, S., 1989. Drag and reconfiguration of broad leaves in high winds. J. Exp. Bot. 40, 941–948.

Vogel, S., 2009. Leaves in the lowest and highest winds: temperature, force, shape. New Phytol. 183 (1), 13–26.

Zhao, Y.P., Li, Y.C., Dong, G.H., Gui, F.K., Teng, B., 2007. Numerical simulation of the effects of structure size ratio and mesh type on three-dimensional deformation of the fishing-net gravity cage in current. Aquac. Eng. 36, 285–301.